RM No. L6J18b

NACA

RESEARCH MEMORANDUM

INFLUENCE OF WALL BOUNDARY LAYER UPON THE PERFORMANCE OF AN AXIAL-FLOW FAN ROTOR

By

Emanuel Boxer

Langley Memorial Aeronautical Laboratory
Langley Field, Va.

CLASSIFIED DOCUMENT

This document contains classified information affecting the National Defense of the United States within the meaning of the Espionage Act, USC 50:31 and 32. Its transmission or the revelation of its contents in any manner to an unauthorized person is prohibited by law. Information so classified may be imparted only to persons in the military and naval services of the United States, appropriate civilian officers and employees of the Federal Government who have a legitimate interest therein, and to United States citizens of known loyalty and discretion who of necessity must be informed thereof.

NATIONAL ADVISORY COMMITTEE
FOR AERONAUTICS

WASHINGTON

May 19, 1947

NATIONAL ADVISORY COMMITTEE FOR AERONAUTICS

RESEARCH MEMORANDUM

INFLUENCE OF WALL BOUNDARY LAYER UPON THE PERFORMANCE OF AN AXIAL-FLOW FAN ROTOR

By Emanuel Boxer

SUMMARY

An experimental investigation has been conducted to determine the effects of the wall boundary layer upon the performance of an axial-flow fan rotor. Tests were conducted at low Mach numbers and at one blade angle on a fan designed to have uniform downstream tangential velocity. The maximum disturbed flow region of the six boundary-layer configurations tested exceeded one-half of the annular width of the duct, and the peak efficiency was reduced $2\frac{1}{2}$ percent for this condition. The over-all loss in efficiency may possibly be reduced by decreasing the blade pitch angle in the boundary-layer region to conform to the upstream velocity profile.

INTRODUCTION

In the design of axial-flow fan and compressor rotors the retardation of flow in the boundary layer is generally ignored; the axial velocity upstream of the rotor is assumed to be constant from wall to wall. Calculations, based upon this assumption and upon appropriate cascade data, yield results that are in good agreement with experimental results obtained in previous laboratory investigations (references 1, 2, and 3), which were made under nearly ideal conditions (that is, uniform axial velocity and minimum blade-tip clearance and boundary-layer thickness). Ideal conditions are seldom encountered, however, in actual axial-flow-fan or compressor installations because duct bends and long rough-jointed expanding ducts materially affect the flow pattern. In addition, the three-dimensional effect of the high-pressure-rise rotor and the tip-clearance effects tend to increase the boundary-layer thickness through several stages of a compressor. (See reference 1.)

Although the efficiency decrement caused by increasing the tip clearance has been determined for specific fans (references 1 and 3), no data are available on the effects of wall boundary layer

upon fan performance. The present investigation was therefore undertaken to determine experimentally the effects of wall boundary layer upon the operating characteristics of an axial-flow fan rotor. The tests were made in the Langley propeller-research-tunnel laboratory at low Mach numbers, with one blade design at one blade angle, and for six boundary-layer configurations; the maximum thickness of the disturbed flow region on one wall was approximately one-third of the duct annular width.

SYMBOLS AND COEFFICIENTS

D inside diameter of fan casing, feet

H total pressure, pounds per square foot

ΔH total-pressure rise, pounds per square foot

$\overline{\Delta H}$ weighted average total-pressure rise, pounds per square foot

$$\left(\pi \int_{r_h}^{r_t} \left(\frac{H_2 V_{a_2}}{Q_2} - \frac{H_1 V_{a_1}}{Q_1} \right) dr^2 \right)$$

n rotational speed, revolutions per second

Q quantity rate of flow, cubic feet per second

q_a axial dynamic pressure of fan, pounds per square foot

r radius, feet

R radius to fan casing, feet

T torque, pound-feet $\left(\pi \int_{r_h}^{r_t} \rho_2 u_2 V_{a_2} r \, dr^2 \right)$

u absolute tangential velocity, feet per second

V absolute velocity, feet per second

V_a axial velocity of air, feet per second

y radial distance from wall, inches

β stagger angle; angle between effective relative entering air and fan axis, degrees (see fig. 1, also reference 1)

δ boundary-layer thickness, inches

θ effective turning angle, degrees (see fig. 1, also reference 1)

$$\left(\beta - \tan^{-1}\left(\frac{4\pi rn - 2u_2}{V_{a_1} + V_{a_2}}\right)\right)$$

ρ mass density of air, slugs per cubic foot

C_H total-pressure-rise coefficient $\left(\frac{\overline{\Delta H}}{\rho_1 n^2 D^2}\right)$

C_T torque coefficient $\left(\frac{T}{\rho_1 n^2 D^5}\right)$

δ^* displacement boundary-layer thickness, inches

$$\left(\int_0^{\delta}\left(1 - \frac{V_l}{\overline{V}_1}\right) dy\right)$$

Q_1/nD^3 quantity coefficient

$V_l/\overline{V}_1$ ratio of local velocity to mean upstream velocity

η_H total-pressure-rise efficiency $\left(\frac{1}{2\pi}\frac{C_H}{C_T}\frac{Q_1}{nD^3}\right)$

$\Delta\eta_H$ loss in total-pressure-rise efficiency, percent

Subscripts:

a axial

h hub

t tip

1 upstream of fan

2 downstream of fan

Bar over symbol indicates an average value.

APPARATUS AND METHODS

The test setup shown schematically in figure 2 has been completely described in reference 1. The instrumentation and equipment is the same as that used in reference 1 with the exception of the spoilers (fig. 3). These spoilers, made of $\frac{1}{16}$-inch aluminum sheet, projected $\frac{1}{8}$ inch and $\frac{1}{4}$ inch from the duct walls and were located $3\frac{1}{2}$ blade chords upstream of the rotor center line. The fan blades shown in figure 4 are the blades used in fan 1 of reference 1; these blades were designed to yield uniform tangential velocity. The blade-angle setting was increased 5° beyond the design point to a value of 50° at the hub section for the present tests.

The testing procedure was identical with that of reference 1. At a fan rotational speed of 3020 rpm (within ±10 rpm) measurements were made of the total and static pressures and of flow angles upstream and downstream of the fan rotor at 20 to 28 radial survey positions. The throttle was adjusted to vary the flow in six approximately equal increments between wide-open throttle and surge. The test readings were converted to the fan coefficients given in the list of symbols.

Tests were made first without spoilers to determine the basic fan performance characteristics; the spoilers then were inserted one at a time on the inner and outer walls. In addition, one series of tests was made with the $\frac{1}{4}$-inch inner spoiler and the $\frac{1}{8}$-inch outer spoiler in place. In all, six boundary-layer configurations were tested.

BOUNDARY LAYER THICKNESS

The velocity profile of the turbulent boundary layers measured 4 inches downstream of the spoilers is shown in figure 5 for the maximum air-flow condition. The scale used in this figure is for convenience in indicating the distance from either wall. A disturbed region of flow approximately one-third of the duct annular width was caused by each of the $\frac{1}{4}$-inch spoilers. Since the expected

efficiency loss is a function of both the extent of the boundary layer and the severity of the velocity retardation, the displacement boundary-layer thickness δ^* is considered the prime parameter determining the efficiency loss. The value of δ^* for each boundary-layer condition at the value of Q_1/nD^3 corresponding to peak efficiency is given in the following table:

Condition	δ^* (in.)	
	Inner surface	Outer surface
No spoiler	0.027	0.014
$\frac{1}{8}$-inch spoiler	.069	.060
$\frac{1}{4}$-inch spoiler	.113	.144

The variation of the displacement boundary-layer thickness with Q_1/nD^3 is shown for the condition of the $\frac{1}{4}$-inch outer spoiler at 3020 rpm in figure 6.

RESULTS AND DISCUSSION

Results showing the variation of C_H, C_T, and η_H with Q_1/nD^3 are presented in figures 7 and 8 in the usual dimensionless form. No attempt was made to determine the effect of the boundary layer on the surge point; however, it was observed that with a thickened boundary layer, surging occurred at a slightly higher quantity rate of flow.

Fan Characteristics

The peak fan efficiency is only slightly affected by an increase in wall boundary-layer thickness; a maximum decrease in peak efficiency of $2\frac{1}{2}$ percent is noted (fig. 8) for the condition in which one-half of the rotor blade is operating in a region of reduced velocity. The decrease in efficiency observed with each of the $\frac{1}{8}$-inch spoilers in place is within the accuracy of the tests, which

was estimated at 1 percent. Each of the $\frac{1}{4}$-inch spoilers reduced the peak efficiency slightly more than 2 percent. In most cases the peak efficiency is shifted to lower values of Q_1/nD^3 presumably because a reduction in the over-all flow is necessary to allow the blade elements in the undisturbed flow to operate at the design angles. At the low blade loadings (that is, high values of Q_1/nD^3) the thickest boundary-layer configuration reduced the efficiency approximately 8 percent.

The decrease in the peak efficiency as a function of the total displacement boundary-layer thickness on both walls is shown in figure 9. Because of the scatter of the data, a single curve has been faired through points representing the results of increasing the boundary layer on the inner and outer walls. Caution should be used in extending these preliminary results to estimated losses for other fan designs or to larger values of δ^*.

Increasing the boundary-layer thickness does not materially affect the torque and total-pressure-rise coefficients. In general, for the lesser boundary-layer thicknesses the values of both C_T and C_H increase. With the $\frac{1}{4}$-inch spoiler in place the efficiency decrease is caused mainly by a decrease in C_H.

Radial Surveys

The radial distribution of the stagger and turning angles and of the axial and tangential components of the downstream velocity is presented in figure 10 for a value of Q_1/nD^3 of 0.760. The angles are computed by using the mean axial velocity at each radial station. With the exception of the curves for the no-spoiler condition, the plots have been obtained by interpolating between test points because the quantity rate of flow could not be determined except by integration of the axial velocity. The variation with Q_1/nD^3 of the quantities involved is very nearly linear in the region near the value of 0.760 for Q_1/nD^3.

Inspection of figure 10 indicates that these trends could have been predicted qualitatively. The reduced downstream velocity in the boundary-layer region requires an increase in velocity in the rest of the flow field to maintain the same quantity rate of flow. In terms of stagger angle, the decrease in velocity appears as an increase in the stagger angle, and conversely the stagger angle is reduced in the increased velocity region. The turning angles are relatively unaffected since the increased angle of attack of the blade section, evidenced by an increased value of β, is countered by a decreased capacity of the blade section to turn the air at the

greater stagger angles, that is, the slope of the curve of θ against angle of attack decreases with increasing values of β.

Although the boundary-layer depth was varied considerably, the points near the walls at which the tangential velocity and turning angle decrease rapidly remained fixed. The radial positions of these points apparently are dependent upon the tip clearance (see reference 1) and upon secondary flows at the hub and are not affected by the increased upstream boundary layer. Since the principal rotor losses appear in the region indicated by the rapid decrease in turning angle, the efficiency loss observed with thickening boundary layer may be assumed to be caused by a low lift-drag ratio of the blade sections operating at greater angles of attack in that part of the boundary-layer flow unaffected by tip-clearance and hub effects. The reason for this assumption may be seen in figure 11 in which the results obtained by using the $\frac{1}{8}$-inch outer spoiler are compared with results calculated by using the turning angles given in reference 2 corresponding to the effective stagger angles measured in the present tests. The curves for the total-pressure rise and turning angles show good agreement with the calculated slopes except near the walls (figs. 11(a) and 11(b)). The turning angle tends to increase slightly at the tip in accordance with two-dimensional data before decreasing under the influence of the tip flows (fig. 11(b)). The total-pressure-rise ratio obtained experimentally decreases throughout the outer boundary-layer region although the experimentally obtained turning angle is unaffected until a point closer to the wall is reached. Since the calculated total-pressure rise was computed by use of

$$\frac{\Delta H}{q_{a_1}} = \eta_{H_s}\left(\frac{V_{a_1}}{\bar{V}_{a_1}}\right)^2\left\{\tan^2\beta - \tan^2(\beta-\theta) + \left[\tan\beta - \tan(\beta-\theta)\right]^2\right\}$$

(where the section efficiency η_{H_s} is assumed to be equal to 1.00 and the initial tangential velocity is nonexistent), the air must therefore be less efficiently turned in that part of the boundary layer unaffected by tip-clearance losses. The over-all loss in efficiency caused by the boundary layer may be reduced by decreasing the pitch angle of the rotor blades in the boundary-layer

region if the upstream velocity profile is known. The blade sections would then operate near the design angle of attack at the design condition.

Langley Memorial Aeronautical Laboratory
National Advisory Committee for Aeronautics
Langley Field, Va.

REFERENCES

1. Kahane, A.: Investigation of Axial-Flow Fan and Compressor Rotors Designed for Three-Dimensional Flow. NACA RM No. L7D02a, 1946.

2. Bogdonoff, Seymour M., and Bogdonoff, Harriet E.: Blade Design Data for Axial-Flow Fans and Compressors. NACA ACR No. L5F07a, 1945.

3. Ruden, P.: Investigation of Single Stage Axial Fans. NACA TM No. 1062, 1944.

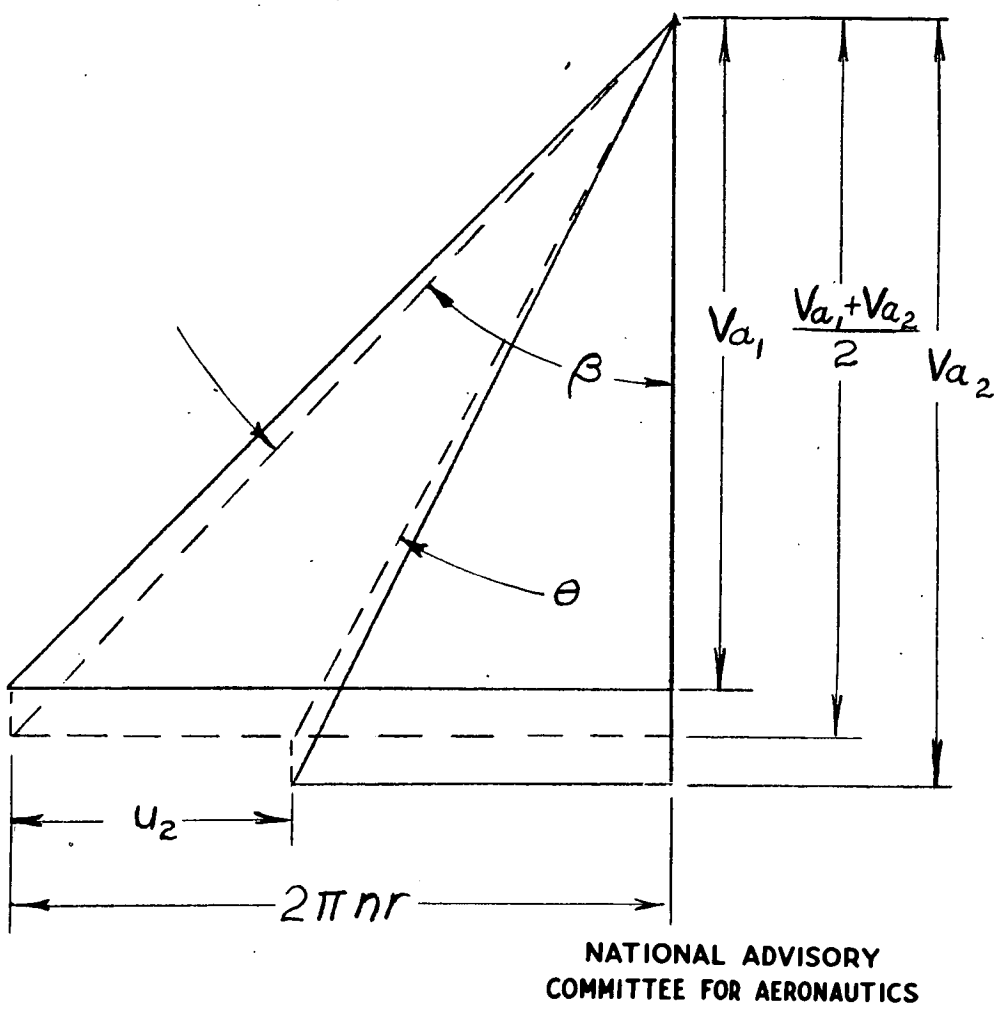

Figure 1.- Typical relative velocity diagram.

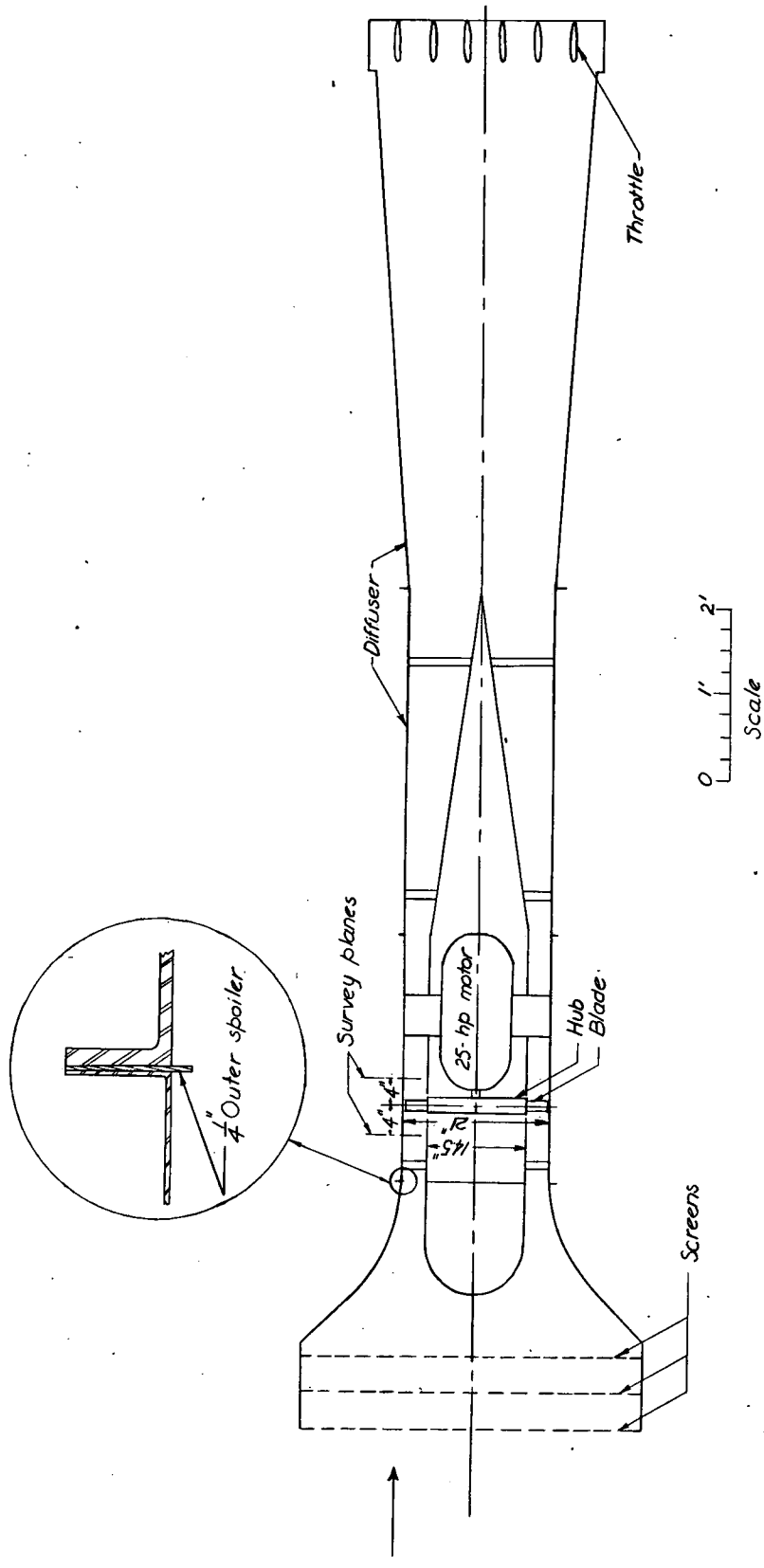

Figure 2.- Schematic drawing of test arrangement.

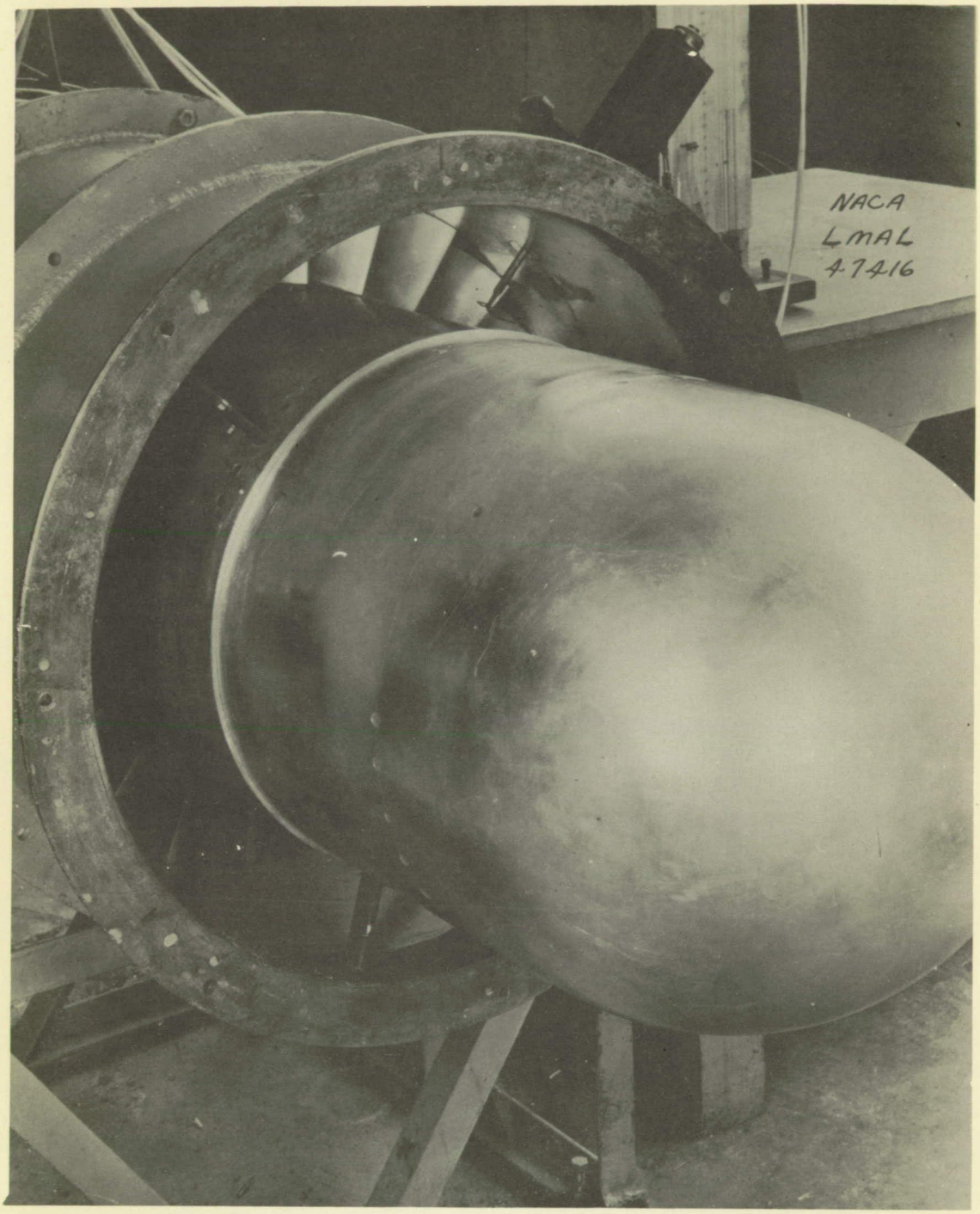

Figure 3.- View of fan showing $\frac{1}{4}$-inch inner spoiler.

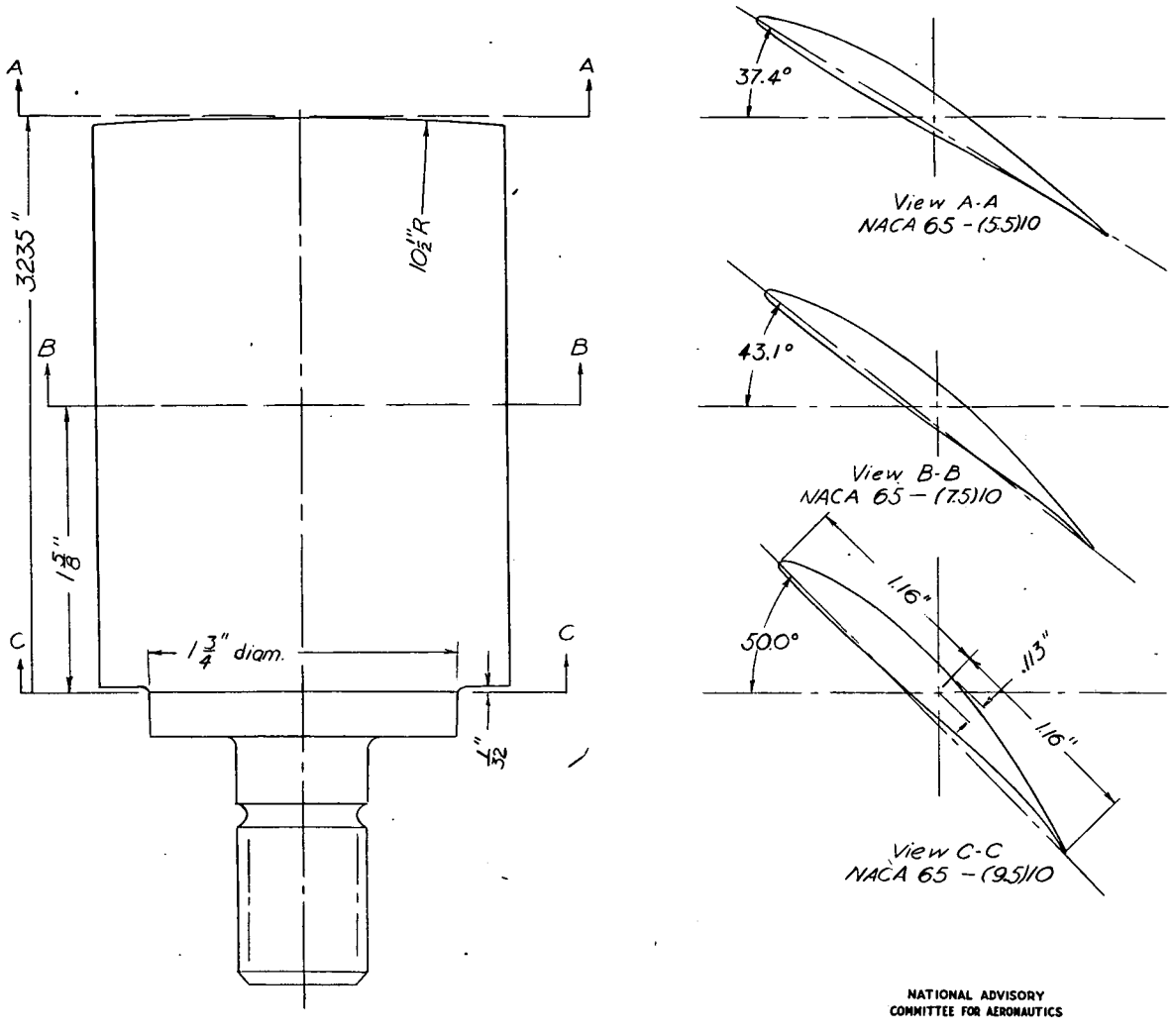

(a) Plan form. (b) Fan blade sections.

Figure 4.- Drawing of rotor blades.

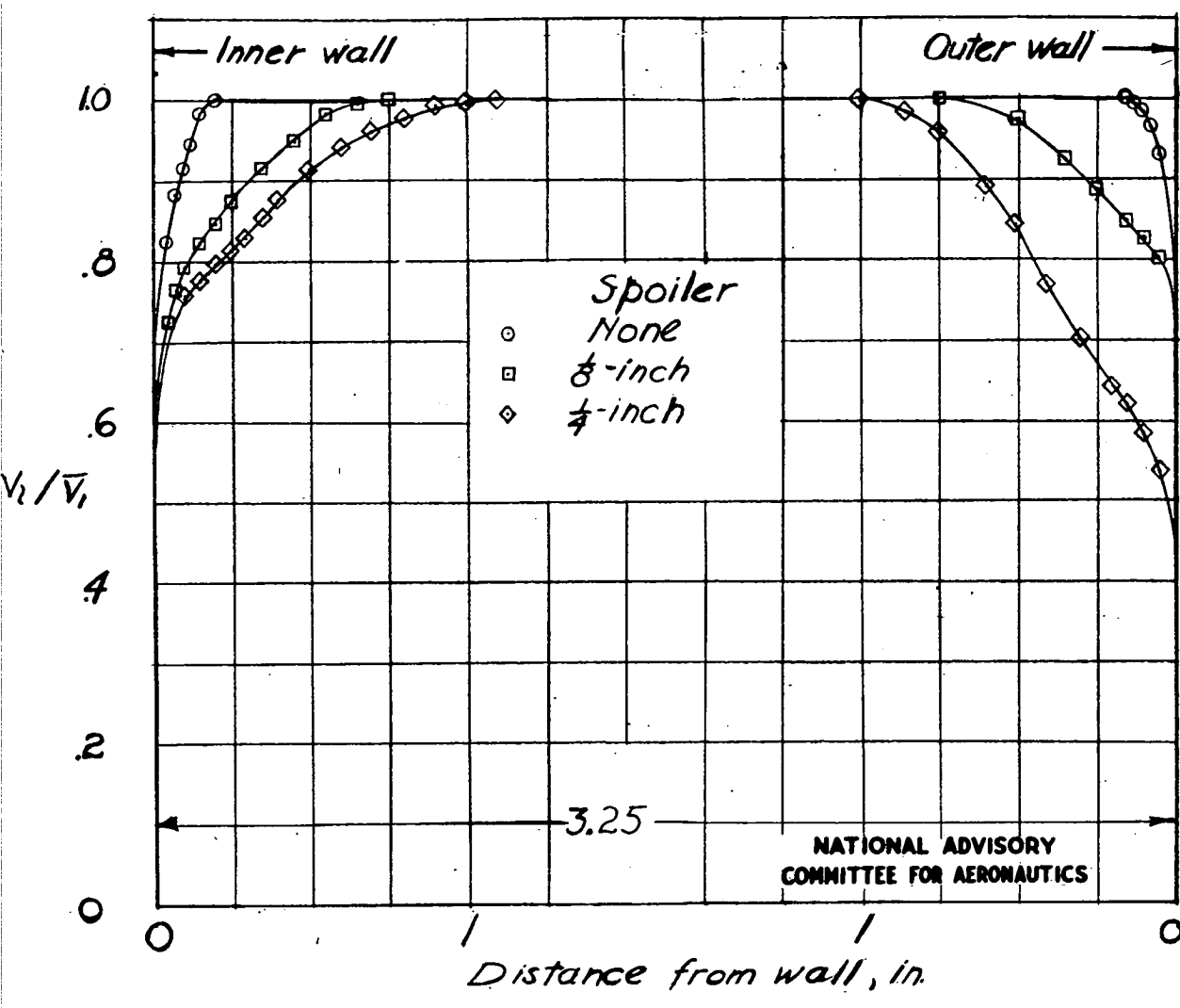

Figure 5.- Boundary-layer profiles upstream of fan.
Maximum air-flow condition.

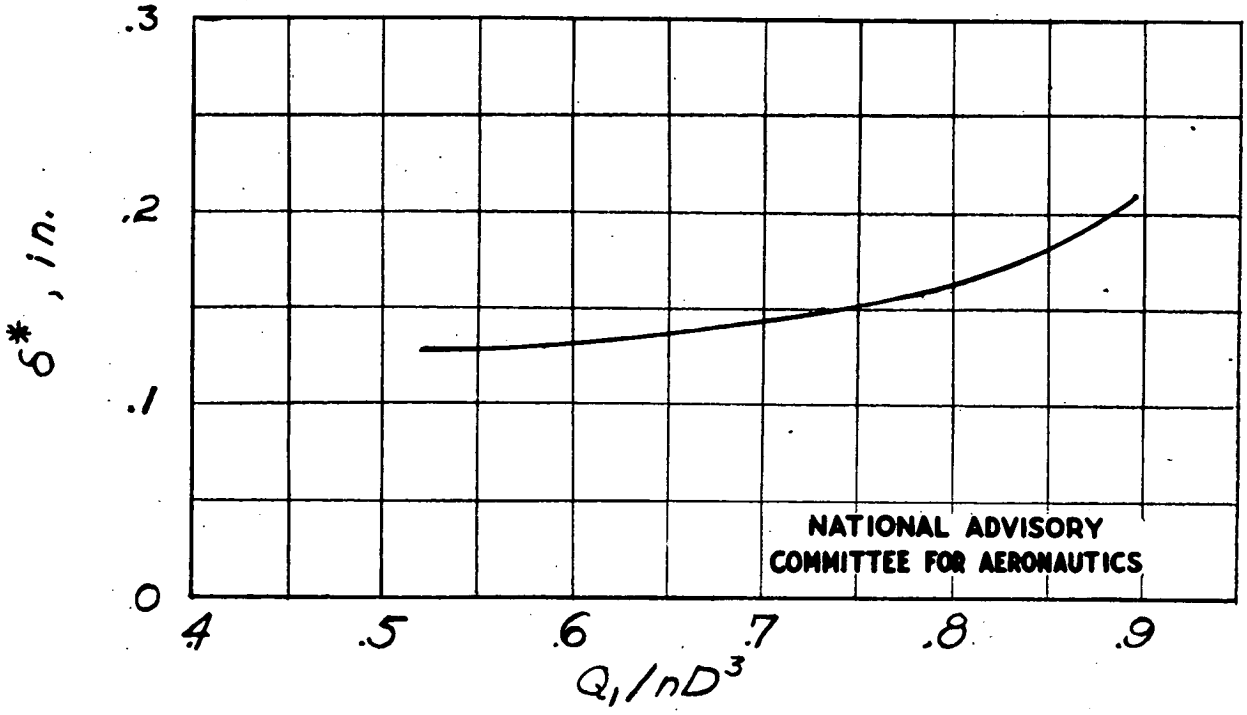

Figure 6.- Variation of δ^* with Q_1/nD^3 upstream of fan Rotational speed, 3020 rpm; $\frac{1}{4}$-inch outer spoiler.

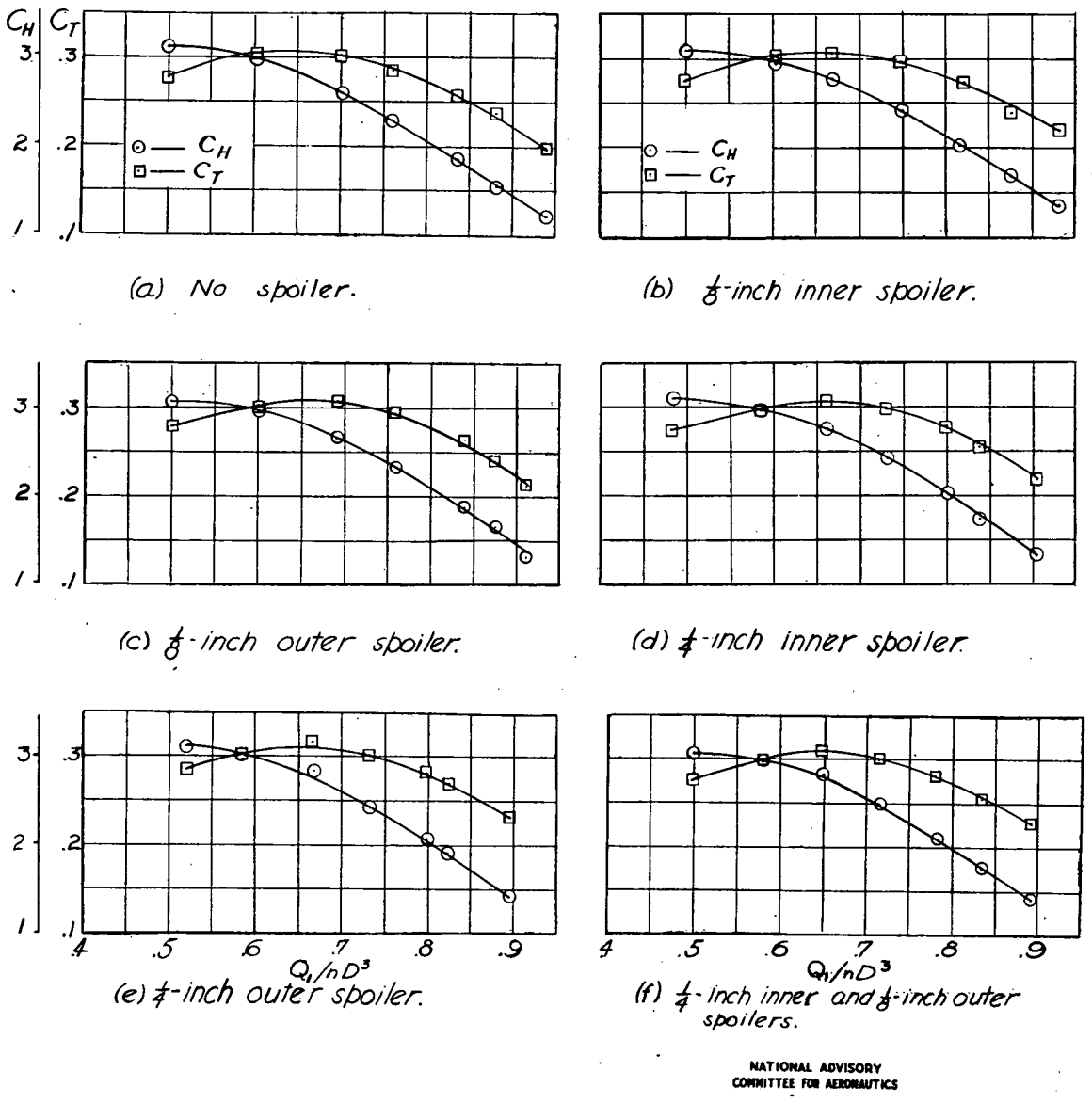

(a) No spoiler.

(b) ⅛-inch inner spoiler.

(c) ⅛-inch outer spoiler.

(d) ¼-inch inner spoiler.

(e) ¼-inch outer spoiler.

(f) ¼-inch inner and ⅛-inch outer spoilers.

NATIONAL ADVISORY COMMITTEE FOR AERONAUTICS

Figure 7.- Total-pressure-rise and torque characteristics.

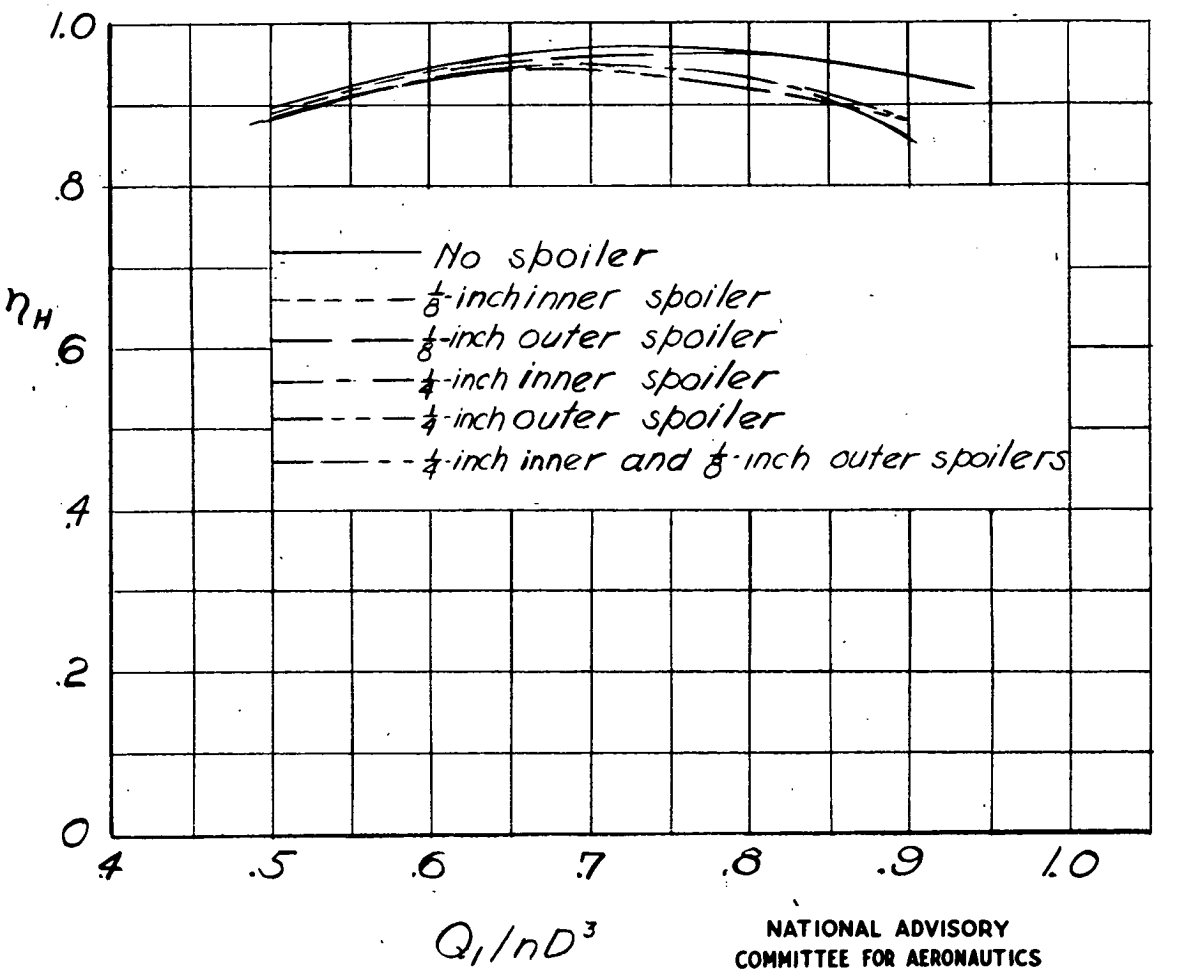

Figure 8.- Fan efficiencies.

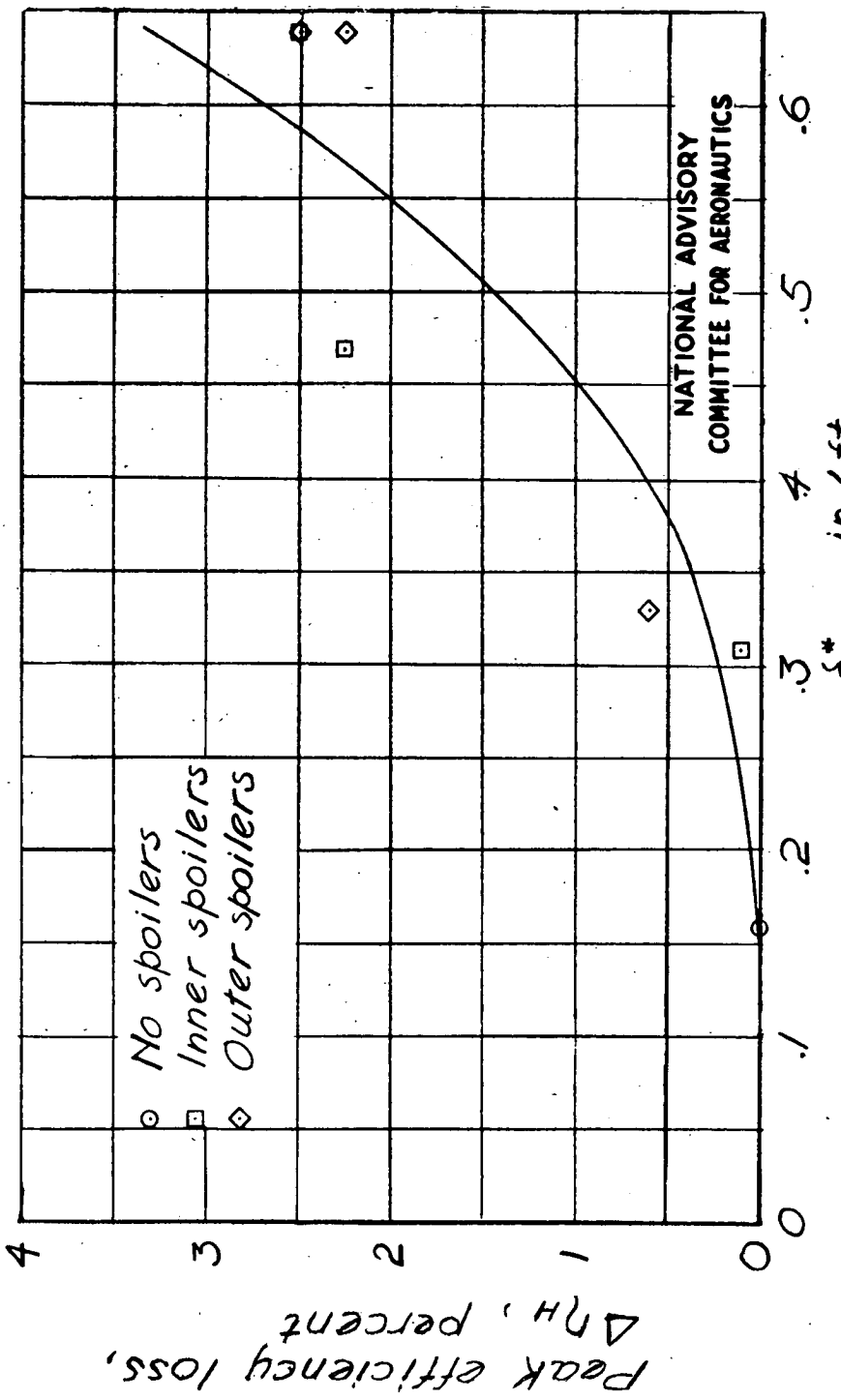

Figure 9.- Peak total-pressure-rise efficiency loss as a function of the total displacement boundary-layer thickness on both walls. Losses are referred to no-spoiler condition.

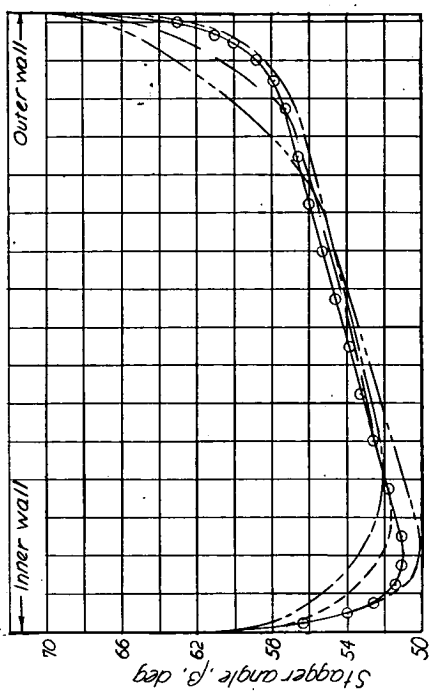

(c) Stagger angle.

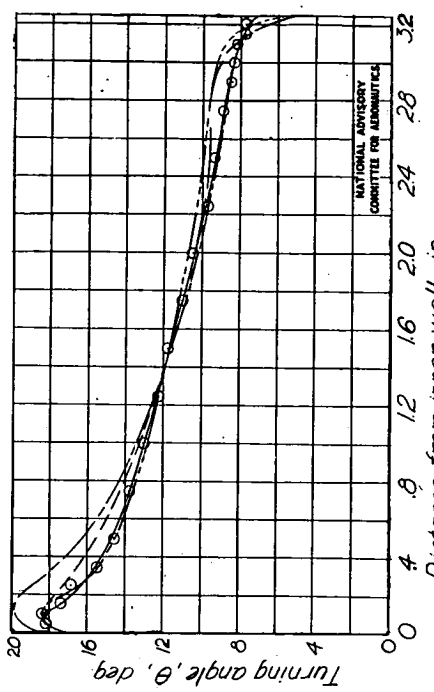

(d) Turning angle.

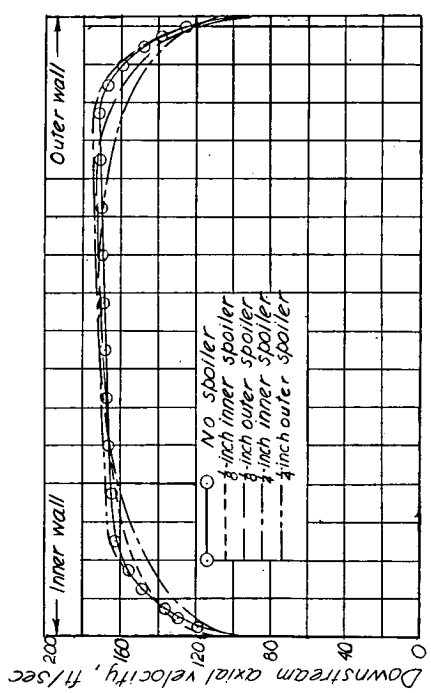

(a) Downstream axial velocity.

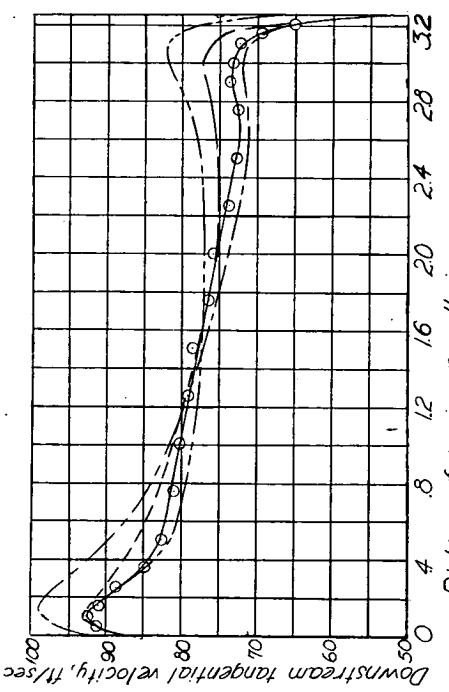

(b) Downstream tangential velocity.

Figure 10.- Results of radial surveys. $\frac{Q_1}{nD^3} = 0.760$.

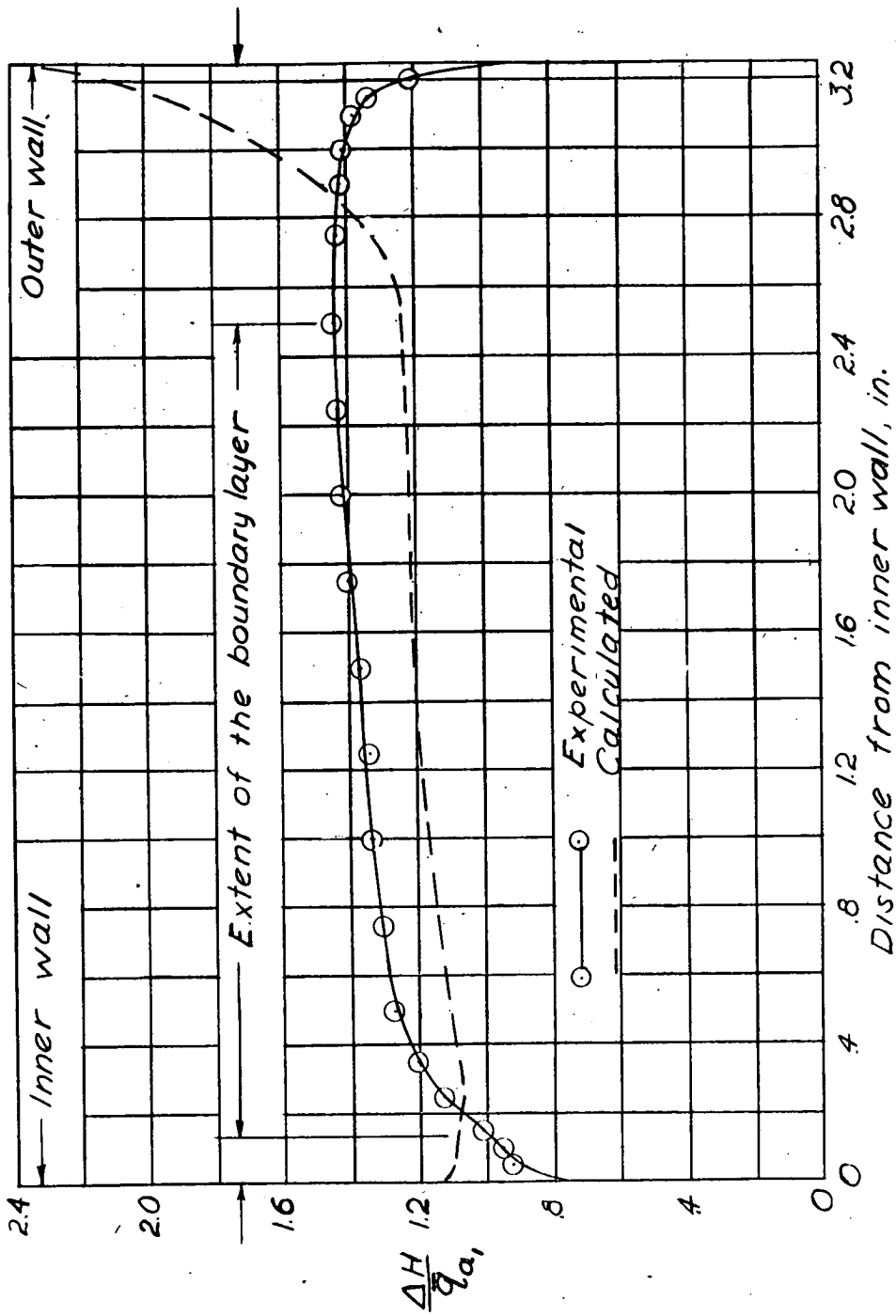

(a) Total-pressure rise.

Figure 11.- Comparison of experimental and calculated data. $\frac{1}{8}$-inch outer spoiler; $\frac{q_1}{nD^3} = 0.759$.

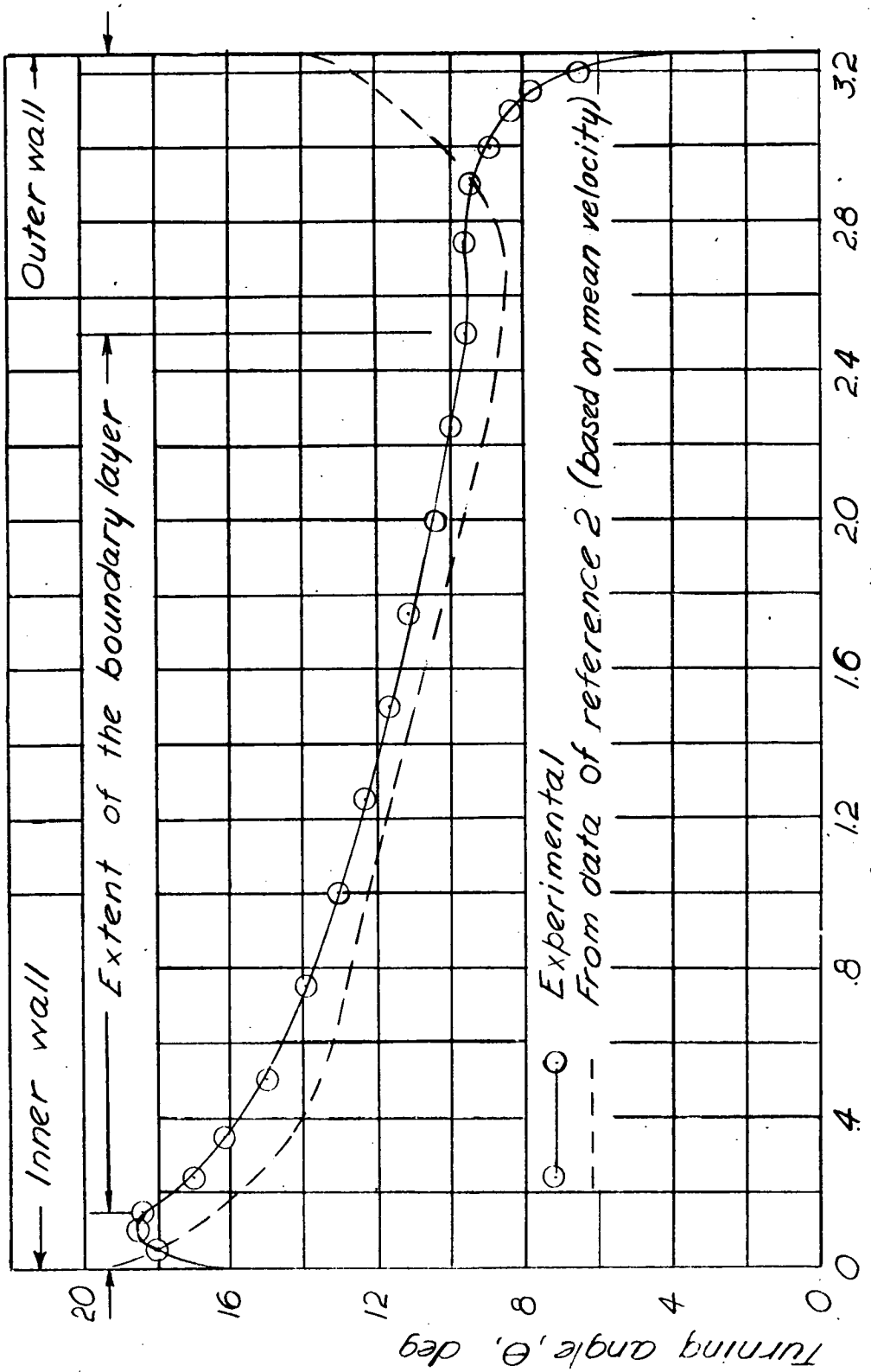

(b) Turning angles.

Figure 11.- Concluded.